Planetary Astrophysics

Planetary Astrophysics

By

Francesco Marzari

Cambridge
Scholars
Publishing

Planetary Astrophysics

By Francesco Marzari

This book first published 2023

Cambridge Scholars Publishing

Lady Stephenson Library, Newcastle upon Tyne, NE6 2PA, UK

British Library Cataloguing in Publication Data
A catalogue record for this book is available from the British Library

ISBN (10): 1-5275-0118-3
ISBN (13): 978-1-5275-0118-8

TABLE OF CONTENTS

PREFACE

Different physical mechanisms are involved in the process of planet formation, starting from the evolution of the dust and gas in a circumstellar disk to the growth of pebbles and planetesimals, which finally accumulate into planets. These mechanisms lead to a very diverse population of planets present in our solar system and in the vast number of extrasolar planetary systems recently discovered. Additional physical processes influence the interaction of planets with their environment and the central star. The presence of a magnetic field is, for example, an essential ingredient for the habitability of a planet, which will be protected by the stellar wind. In this book I try to give a comprehensive outline of all these physical mechanisms involved in sculpting a planetary system and its environment. The most relevant are gravitational and tidal interactions, absorption and re-emission of the star light, magnetic fields and their interaction with the solar wind and the dynamics of fluids, which govern the evolution of circumstellar disks. An effort has been devoted to outline their mathematical aspects and their implications in determining the observed physical and dynamical properties of the known planetary systems. Only essential references are given, quoting the authors of a scientific paper whenever a figure is taken from it. Most topics are part of the lecture notes from the course “Planetary Astrophysics” at the University of Padova in Italy, and it is intended for graduate and post-graduate students and researchers who are new to the field.

1

THE SOLAR SYSTEM

1.1 The context

The solar system is the best known planetary system, where the planets can be reached from Earth with space probes and observed at high resolution from the ground. It is also the test bench that has allowed to develop the standard model for planet formation, further improved following the discoveries of exoplanets. It formed about 4.5 billion years ago and, in addition to planets, it includes asteroids, comets, satellites and dust. The interplanetary space is also filled by the solar wind and by the magnetic fields of the planets.

1.2 The solar system population

The solar system is populated by eight planets: Mercury, Venus, Earth and Mars, known as terrestrial planets, Jupiter and Saturn, the giant planets, and Uranus and Neptune, the icy planets. There are some dwarf planets like the former asteroid Ceres in the asteroid belt and Pluto, Sedna, Haumeamea and others in the Kuiper belt. Most planets have moons with mass ratios ranging from 0.117 (the Pluto–Charon system), 0.0123 (the Moon–Earth system) down to smaller values. The solar system is also populated by minor bodies that are believed to be the remnant of the building blocks of planets, the planetesimals. These planetesimals are divided into two belts: the asteroid belt located roughly between 2.1 to 3.5 *au* with an estimated total mass of $5 \times 10^{-4} M_{\oplus}$, and the Kuiper belt stretching beyond the orbit of Neptune at 30 *au* to an orbital distance of more than 100 *au* from the sun with an estimated mass of $2 \times 10^{-2} M_{\oplus}$. Additional minor bodies are found in Trojan orbits (see Chapter 7.4 and 7.5) around planets Mars, Jupiter and Neptune, in orbits crossing those of the terrestrial planets, the NEOs (near earth object), and in transition orbits from the Kuiper belt into the short period comet population, the Centaurs. The space among the planets is also filled with interplanetary dust particles mostly produced by collisions in the asteroid and Kuiper belts, by

cometary activity and with a limited fraction coming from outside the solar system. Due to the Poynting–Robertson drag (see Chapter 4), these particles spiral towards the sun on timescales that depend on their size and distance from the star. However, collisions and cometary activity constantly refill the dust population which, observed far out of the solar system, would appear as a debris disk with a warm (the asteroid belt) and a cold (the Kuiper belt) component.

	a	T	m	n. satellites	Rot. Per.	ρ
Mercury	0.39	0.24	0.055	0	58.76	5429
Venus	0.72	0.62	0.82	0	-243.69	5243
Earth	1.00	1.00	1.00	1	1.00	5513
Mars	1.52	1.88	0.11	2	1.03	3934
Ceres	2.77	4.60	0.00015	0	0.38	2162
Jupiter	5.20	11.86	317.83	92	0.42	1326
Saturn	9.57	29.42	95.16	83	0.45	687
Uranus	19.19	83.75	14.54	27	-0.72	1270
Neptune	30.18	163.72	17.15	14	0.67	1638
Pluto	39.48	247.94	0.0022	5	-6.41	1854

Table 1: main properties of the eight planets and of two dwarf planets (Ceres and Pluto). The number of satellites is given at the present date. The semi-major axis a is in au, the orbital period T in years, the mass m in Earth masses, the rotation period in days (negative for retrograde rotation) and the density ρ in kg/m^3. Data are taken from the NSSDCA-NASA archive.

In Table 1 are listed the main physical and dynamical properties of the planets. It is noteworthy that the terrestrial planets are concentrated in the inner region, within 1.5 au, while the giant and icy planets are found beyond 5 au. In addition, there is a correlation between the radial distance and the planet densities, with the denser planets populating the inner region. These two features are related to the process of planet formation.

1.3 The standard model of planet formation

The planet formation model, developed to explain the architecture of the solar system, is called the *standard model* and it consists of six main steps:

1) A protostellar cloud, or part of it, collapses into a protostar.
2) A circumstellar disk made of gas and dust forms around the protostar due to the conservation of angular momentum.
3) Pebbles and planetesimals grow from the dust in the disk.

4) Planetesimals and pebbles accumulate into planetary embryos.
5) Terrestrial planets and the core of giant planets grow from collisions between planetary embryos with an additional contribution from the accumulation of leftover pebbles and planetesimals.
6) A large amount of gas collapses on the core of giant planets like Jupiter and Saturn.

1.4 Circumstellar disks, the cradles of planets

A disk of rotating circumstellar material (gas and dust) usually forms around a growing protostar as a consequence of angular momentum conservation during cloud collapse. The initial stages of the disk are quite turbulent due to infall of material on the disk. This period is followed by a quieter state, during which the dust settles towards the middle plane of the disk (see Chapter 5.10). A radial temperature gradient is present in the disk due to viscous heating, which causes higher temperatures in the inner regions because of a stronger Keplerian shear (see Chapter 11.5). The so-called "snow line" or "frost line" marks the radial distance at which the disk temperature drops below the condensation temperature of a particular ice (H_2O, CO_2, CO, CH_4, NH_3). For example, the "frost line" of water ice is located around 3–5 *au* for circumstellar disks around solar type stars, while the carbon dioxide, methane and carbon monoxide lines are located outwards at lower temperatures. Circumstellar disks around stars have been detected with different methods, either with the infrared excess in the power spectrum of a star or via direct imaging with high-resolution instruments (HST, ALMA, SPHERE …). If a circumstellar disk is present around a star, its dust emits at a lower temperature with respect to the star and its blackbody radiation falls within the infrared spectral range (see Appendix C). As a consequence, the observed spectrum of the star is given by the combination of that of a blackbody with a superficial temperature of about 6,000 *K* (for solar-like stars) and that of a colder source (the disk) with a temperature below 1,000 *K*, the infrared excess. In Fig. 1 an example of infrared excess in the spectrum of a star is shown. If we imagine to divide the disk in rings with different temperatures, it is possible from the morphology of the infrared excess to deduce if the disk has gaps or an inner hole like in transition disks.

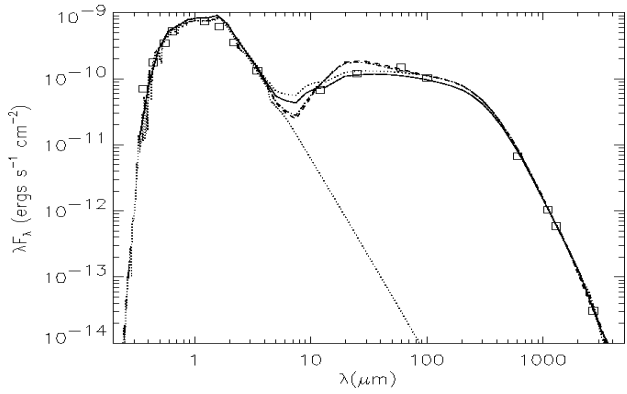

Fig. 1: Power spectrum, also known as SED (spectral energy distribution), of GM Aurigae, a classical T Tauri star. It shows a large mid- to far-infrared excess indicating the presence of a circumstellar disk. The shape of the infrared emission can give insights on the disk properties (Schneider et al., 2003).

From the shape of the infrared excess it is possible to derive approximate radial profiles of the surface gas density distribution Σ (see Chapter 11.5) and temperature T. A power law is usually adopted to model both

$$\Sigma(\mathrm{R})=\Sigma_0\left(\frac{R}{R_0}\right)^{-q} \qquad \Sigma_0 \approx 10^2 - 10^4\ g/\mathrm{cm}^2 \qquad \mathrm{q} \approx\ 1/2 -\ 3/2$$

$$T(R)=\mathrm{T}_0\left(\frac{R}{R_0}\right)^{-p} \qquad T_0 \approx 1000 - 2000K \qquad \mathrm{p} \approx\ 1/2 -\ 1$$

where R is the radial distance and R_0 a reference distance typically equal to 1 *au*. By fitting the observed infrared excess, approximate values for Σ_0, T_0, q, p can be extrapolated. A typical reference disk is the so-called Minimum Mass Solar Nebula (MMSN), whose density profile is

$$\Sigma(R) = 1700\frac{g}{cm^2}\left(\frac{R}{1au}\right)^{-3/2}$$

giving a total mass in the disk of $M_d \sim 0.01 M_{sun}$. The MMSN density profile is obtained by smearing the mass of the planets on a disk extending approximately for 40 *au* and reconstructing the gas density assuming a dust-to-gas ratio of 0.01 (the classical interstellar value). Recently, on the basis of the characteristics of extrasolar planetary systems, in particular

those packed and close to the star, more massive disks are suggested (Minimum Mass Extrasolar Nebula, MMEN) with values of Σ_0 ranging from 5 to 20 times that of the MMSN. With the arrival of ALMA (Atacama Large Millimeter Array), high-resolution images of circumstellar disks have become possible. They highlight many different features in disks like gaps, spiral waves and inner holes (see Fig. 2). Thanks to the capability of ALMA, it has also been possible to image a large sample of disks within different stellar clusters and star-forming regions, obtaining statistical estimates of the mass in the disks as a function of the cluster age, as in Fig. 3. The average disk mass in the older regions is significantly lower than that in the younger ones, showing that disks dissipate on a timescale of some Myrs.

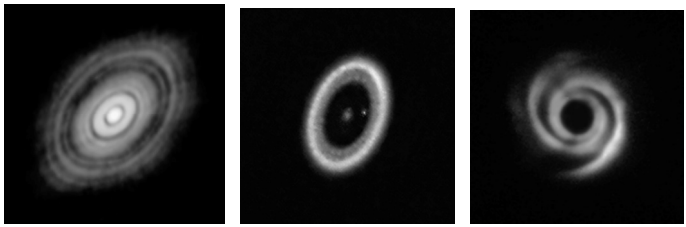

Fig. 2: Three examples of circumstellar disks imaged with ALMA. The first on the left is the disk around HL Tauri, that in the middle is the disk of PDS 70 with the glimpse of a growing planet, the one on the right is that around HD 135344B (credit: ALMA, ESO/NAOJ/NRAO).

The two most important mechanisms for disk dissipation are viscous accretion and photoevaporation. The detection of an ultraviolet and optical excess in the spectrum of a star confirms that there is mass accretion on the star surface due to disk mass infall (see Chapter 11.6). This is illustrated in Fig. 4 where the photospheric emission at small wavelength (the bottom solid line) is overcome by the emission of the shock wave produced by disk material impacting the surface of the star. This is strong evidence of the viscous evolution of a disk causing a transfer of angular momentum towards the outer regions and an inward flux of disk mass towards the star. At the inner edge of the disk the gas is ionized and it follows the dipolar magnetic field lines of the star down to its surface. An additional mechanism favoring the disk dissipation is photoevaporation driven by FUV (far ultraviolet), EUV (extreme ultraviolet) radiation and X-rays. These radiations are produced in the stellar chromosphere and cause photoevaporative winds in the upper layers of the disk eroding it.

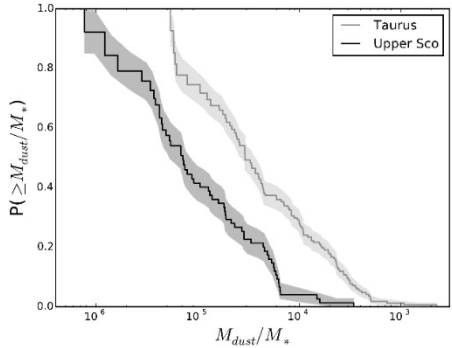

Fig. 3: Cumulative distribution of the dust-to-star mass ratio in the Taurus star forming region (age 1-2 *Myr*) and the in Upper Scorpius association (age 5-11 *Myr*). There is a significant decrease in the mass of the disks of the older cluster, a clear sign of erosion with age (Barenfled et al., 2016).

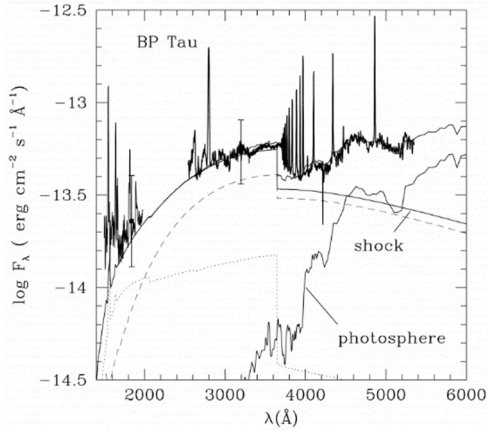

Fig. 4: Ultraviolet spectrum of pre-main-sequence star BP Tau. The thick solid line is the observed spectrum while the thin solid line is the theoretical model. It is obtained by adding the emission from the shock due to the impact of the disk material on the star surface and the emission from the stellar photosphere (Gullbring et al., 2000).

An additional way to estimate the timescale for disk dispersal is to derive the fraction of disk-bearing stars in different clusters. The outcome of these observations is plotted in Fig. 5 where the fraction of stars with a

disk is plotted vs. the age of the cluster, giving a strong indication that after 10 *Myr* most of the disks have been dispersed.

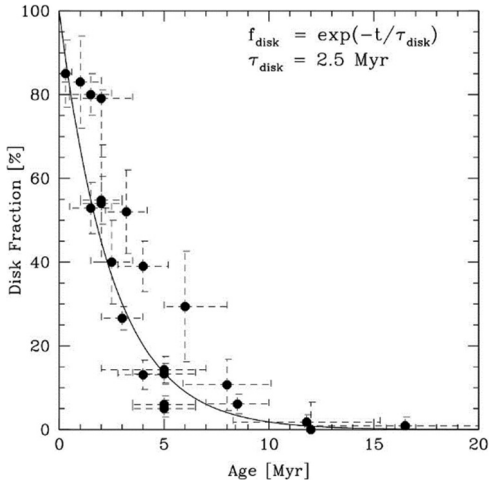

Fig. 5: Fraction of stars with disks (identified in most cases by the infrared excess in the SED) as a function of the cluster age (Mamajek, 2009).

1.5 Pebble and planetesimal formation

During the quiet phase, the dust settles towards the middle plane of the disk and it grows into larger bodies. There is a theoretical transition from dust particles and pebbles to planetesimals, which occurs when the gas drag is not anymore strongly influencing the evolution of the bodies but it becomes a perturbation of the Keplerian motion (transition from Epstein to Stokes drag; see Chapter 5.10 and 5.12). The transition size for a typical disk is of some kilometers in radius and the bodies of this size cease being "suspended" in the gas and perform elliptical orbits crossing the median plane of the disk. Of course, a sharp cut-off in size is not physical and there will be a slow transition from one kind of motion to the other depending on the radius of the bodies. The planetesimal theory was developed to account for the presence of minor bodies in the solar system, interpreted as remnants of the initial planetesimal population from which the planets formed, and by the observation of debris disks around other stars. In a minor body population, the size distribution is indicative of the growth process that has been interrupted preventing them to form a fully grown planet. In the asteroid belt one hypothesis for the failure of building

up a planet is that the fast growth of Jupiter caused a significant increase in the impact speed between the planetesimals leading to disruptive collisions. An intriguing problem is how planetesimals form from the dust in the disk since it appears to be a path strewn with obstacles. It was believed that the progressive accumulation of dust into larger bodies lead directly to planetesimals via two-body collisions. However, the outcome of a collision can be constructive or erosive, as shown in Fig. 6.

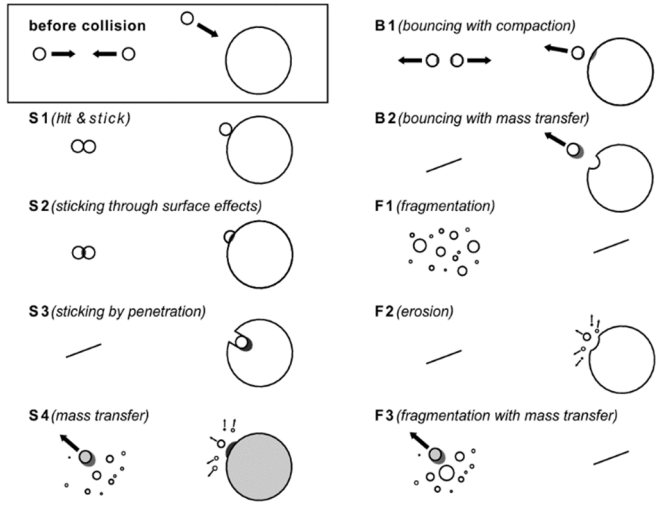

Fig. 6: Possible outcomes of two-body collisions between dust particles of different sizes. On the left side of the plot accreting type of impacts (S-impacts) are illustrated leading to mass growth. On the right side the B-impacts do not cause any change in the mass of the target and projectile while the F-ones are erosive.

If the impact speed is too high, the chemical sticking forces are not strong enough to assemble a bigger body and fragmentation and cratering with mass loss dominate. These last processes halt or even reverse the dust accumulation process. The relative velocity between dust particles is determined by the sum of the following contributions:

1) Brownian velocity, which gives a contribution of the order of the thermal velocity $v \sim v_{th} = \sqrt{\frac{8K_BT}{\pi\mu m_H}}$ with K_B Boltzmann constant, T the local temperature of the gas, μ the mean molecular weight (~ 2.35) and m_H the mass of the hydrogen atom

2) differential vertical settling velocity $v_{\text{settle}} = \frac{\rho_d}{\rho_g}\frac{s}{v_{\text{th}}}\Omega^2 z$ due to the different settling velocities of dust grains of different sizes (see Chapter 5.10), where ρ_d is the density and s the radius of the grains, $\rho_g$the gas density and Ω the Keplerian frequency
3) differential radial drift velocity towards the star $v_{\text{radial}} = -\eta\frac{\rho_d}{\rho_g}\frac{s}{v_{\text{th}}}\Omega^2 R$ where η is a coefficient estimating the difference between the rotating frequency of the gas with respect to the Keplerian one (see Chapter 5.9) and R the radial distance from the star

In addition to these three components, gas turbulence can also give a significant contribution to the impact speed. In Fig. 7 the expected relative velocity is computed as a function of the target and projectile mass by adding up all the above-mentioned contributions. When the size of the dust grains reaches a few centimeters (pebble size), the relative impact velocities have a sudden increase and laboratory experiments show that, for such high-impact velocities, the accretion process halts. There are factors that may enhance the sticking between dust particles like: 1) dipole charging, which may lead to a stronger electrostatic attraction 2) aerodynamical re-accretion, where smaller fragments of a collision feel a stronger gas headwind and are accreted back on the target 3) magnetic sticking 4) compositional features like porosity and ice fraction which may enhance the sticking. However, there is also an additional obstacle to the formation of kilometer-size planetesimals, the meter-size barrier.

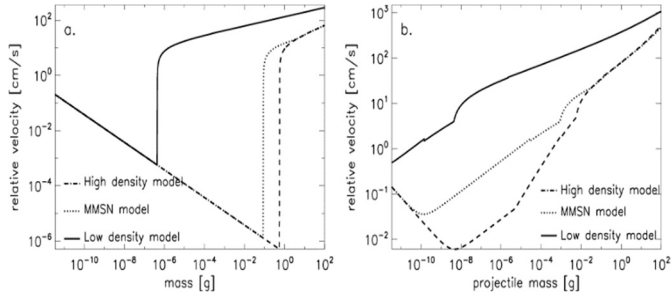

Fig. 7: Relative velocities between dust particles caused by Brownian motion, vertical settling, radial drift, and turbulence in three different disk models for equal-sized particles (panel a) and for different-sized particles with a mass ratio of 100 (panel b) (Zsom et al., 2010).

When the growing bodies become boulder-sized bodies (~1 m), the interaction with the gas component of the disk leads to a fast spiraling towards the star, much faster compared to the drift they experience when they are in the mm to cm-size regime. The inward radial velocity becomes comparable to the Keplerian velocity $v_{radial} \sim -0.5\eta v_K$ and the timescale to drift towards the star can be of the order of 100–1,000 yr. This may prevent further growth of pebbles and boulders into planetesimals. As an alternative to the continuous growth of dust into planetesimals, gravitational instability has been proposed as a possible mechanism to convert directly dust into planetesimals when most of the grains settle in the middle plane of a disk forming a thick dust layer. However, the onset of a Kelvin–Helmholtz instability due to the back-reaction of dust on the gas creates turbulence that diffuses the dust grains along the vertical direction, reducing the density below the value needed for gravitational instability to be effective. An intense photoevaporation may reduce the gas density with respect to that of the dust, allowing the gravitational instability to occur anyway, but this seems unlikely in the initial phases of evolution of a disk when planetesimals are supposed to form. The development of pressure bumps (see Chapter 5.11) can lead to dust concentration and planetesimal formation. These pressure bumps can be related to the formation of rotating structures due to gas turbulence caused by different sources (magneto rotational instability, baroclinic instability, vertical shear instability, gravitational instability etc.). Different sizes of eddies are expected to form depending on the active contribution of the Coriolis force and Keplerian shear. At the pressure bumps the dust is concentrated up to a value beyond which it collapses into a single body. An additional source of instability leading to passive concentration of dust grains is streaming instability due to the back-reaction of the dust on the gas, which leads to the formation of high-density filaments in the gas, which trap the dust and may lead to the formation of fluffy planetesimals. However, streaming instability efficiency depends on the initial particle size distribution (it must be concentrated in pebbles) and on the dust-to-gas ratio, which requires photo-evaporation to become large enough to lead to planetesimal formation. Particle concentration due to gas instabilities may lead to the formation of 50–100 km planetesimals, which would subsequently grow by mutual collisions with gravity-granting accretion-only impacts. It might also explain the occurrence of many equal-sized binaries in the Kuiper belt. Additional more localized dust traps can be produced by the formation of dead zones in the disk, where the gas ionization is too low to allow the onset of significant viscosity, assuming that magneto rotational instability is indeed responsible for the

viscosity of the disk. At the transition edge of a dead zone a gas bump forms where the dust particles cluster and may grow into planetesimals. The same may happen near a frost line, either for water, ammonia, methane or carbon dioxide/monoxide. Large grains coming from outside the frost line shrink due to evaporation after crossing the line. This causes a slowdown of their inward drift velocity, which depends on the particle size, leading to an increase in the dust density with the potential of forming planetesimals.

1.6 Planetesimal accumulation

The planetesimal accumulation process can be divided into three different stages:

1) Runaway growth: some planetesimal outrun the others and grow at a faster pace becoming protoplanets of Lunar to Martian mass (at 1 *au* from the star). This is shown via numerical modeling in Fig. 8.

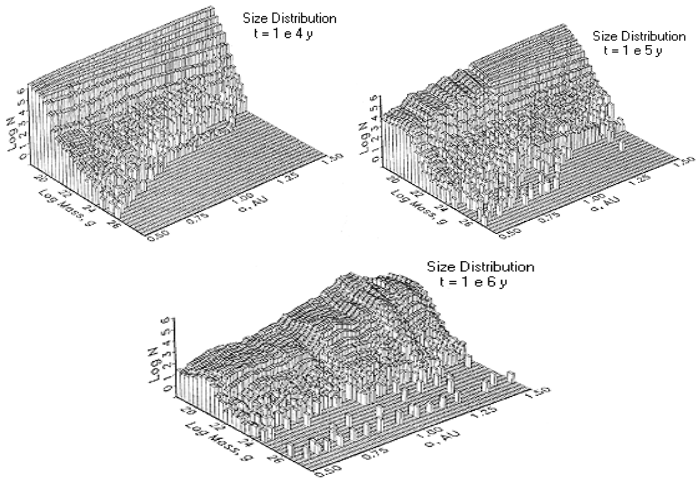

Fig. 8: Planetesimal accumulation modelled with the planet-building code (Weidenschilling et al., 1997). An initial population of planetesimals is evolved through collisions until runaway growth occurs after approximately 1 *Myr*. On the *x*-axis there is the distance of the planetesimals from the star, on the *y*-axis their mass and on the *z*-axis the number of bodies with the values of mass and radial distance given in the *x,y*-axes.

2) Oligarchic growth: it occurs when the runaway protoplanets become massive enough to affect the planetesimals random velocities by increasing their eccentricities and inclinations. The transition typically takes place when the mass of the protoplanets exceeds 100 times the average mass of planetesimals. The growth rate of the protoplanets decreases in this regime because of the greater relative velocities between the protoplanet and planetesimals even if the mass ratio of the protoplanets to the planetesimals continues to increase with time. The protoplanets keep a typical mutual orbital separation of 10 Hill's radius, where the Hill's radius is defined as (see Chapter 7.7)

$$R_H = \left(\frac{m}{3M_s}\right)^{1/3} a$$

with m the mass of the protoplanet, M_s the mass of the star and a the semi-major axis of the protoplanet (see Appendix A for the definition of orbital elements). In this period protoplanets grow "oligarchically" and no substantial accretion between the remaining planetesimals occurs because of their higher impact velocities. The mass distribution becomes bi-modal: a small number of protoplanetary bodies dominate the planetesimal swarm over a large number of small planetesimals, which do not grow anymore. In Fig. 9 the outcome of an N-body numerical simulation illustrates the oligarchic growth phase.

3) Giant impact stage: when there is insufficient damping of the eccentricity of the protoplanets by dynamical friction with smaller planetesimals, the "oligarchs" begin to excite each other's orbits. This typically happens in the terrestrial region of the solar system when the planetary embryos reach a mass of about $0.1\ M_\oplus$. The evolution becomes chaotic, they have frequent close encounters and giant protoplanet–protoplanet collisions occur with the formation of larger bodies like Earth or Venus. Mars could be the remnant of a protoplanet, while Mercury, with its large iron-rich core (about 70% of its mass), could have survived an impact with a larger body that stripped off its mantle during a high-velocity collision in a hit-and-run scenario like that described by Asphaug & Reufer (2014). In this period also the Moon would have formed after an impact of a protoplanet on the almost full-grown Earth.

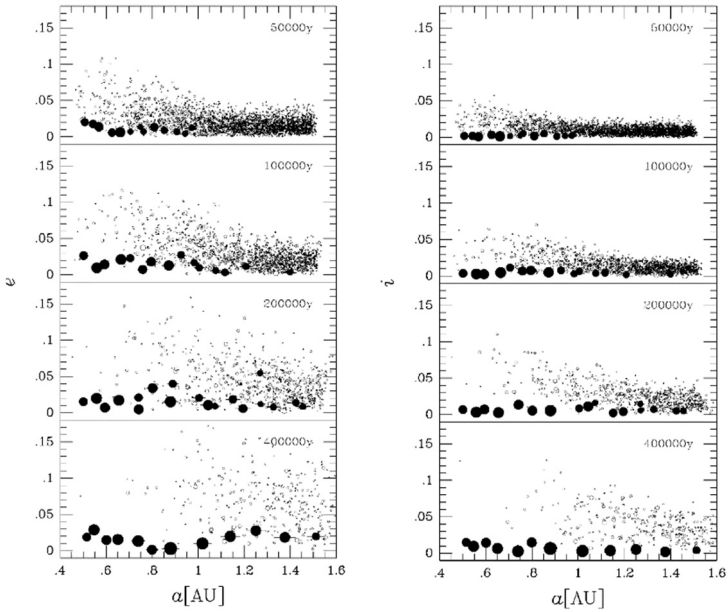

Fig. 9: Example of oligarchic growth in the terrestrial region computed via an N-body numerical simulation (Kokubo & Ida, 2002) in the *a-e* (left panel) and *a-i* (right panel) planes. The initial protoplanets grow by feeding from the leftover planetesimals and a final population of few oligarchs is produced after about $4 \times 10^5 yr$. The circle size of each body is proportional to its radius. The filled circles mark bodies with masses larger than $1.5 \times 10^{26} g$.

1.7 Pebble accretion

Not all the primordial dust in the disk accumulates into planetesimals but, depending on the planetesimal formation process, a significant amount of mass can remain in the form of pebbles, decimeter size rocky-icy bodies. In the presence of gas, they migrate inwards and they approach the growing planetary embryos enhancing their growth rate. The gas drag acting on the pebbles in the proximity of a protoplanet significantly increases the impact rate on it, as shown in Fig. 10. With the help of pebble accretion, the rate of mass growth of protoplanets can be significantly higher than in a planetesimal-only scenario, leading to shorter timescales for the formation of planets and, in particular, of the cores of giant planets, which must reach completion before the dissipation of the gas in the disk. However, two mechanisms halt pebble accretion: 1) the

fast dissipation of the disk gas that drags the pebbles towards a protoplanet and also enhances the protoplanet impact cross-section and 2) the gravitational perturbations of the growing planet that, when it reaches the so-called pebble isolation mass, generate a pressure bump on the disk at the outer edge of the planet orbit, stopping the inward flux of pebbles. When the dust particles approach the gas bump, they slow down their inward drift and definitively stop at the maximum in the gas density (see Chapter 5.11) accumulating at the outer border of the planet orbit without approaching it.

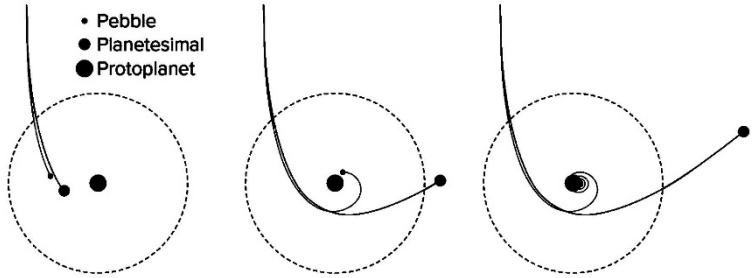

Fig. 10: When pebbles approach a protoplanet, if they are tightly coupled to the gas their impact rate on it is significantly higher than that of planetesimals that follow ballistic impact trajectories (Ormel & Klahr, 2010; Lambrechts & Johansen, 2012).

The pebble isolation mass can range from a few Earth masses to a hundred depending on the disk aspect ratio and viscosity.

1.8 Gas infall onto giant planet cores

The Jupiter and Saturn formation model, termed core-accretion, is based on a sequence of steps. In the initial stage of a giant planet growth, planetesimals accumulate into large protoplanets beyond the frost line where more solid material is available due to the contribution of ices to the rocky material. As a protoplanet gets bigger, also with the aid of pebble accretion, it begins to trap some of the nebular gas, which forms a tenuous envelope around it. In this phase, the mass growth of the protoplanet is still dominated by planetesimal/pebble accretion but the protoplanet is called a core since it will be the solid nucleus of the giant planet. When the planetesimal feeding zone of the core is depleted of planetesimals, it is the gaseous envelope that grows at a faster rate by accreting the surrounding gas. The growth is determined by the contraction of the inner shells of the

gaseous envelope, which frees up space for additional gas, and by the simultaneous mass increase, which expands the gravitational reach of the body. This in turn brings new planetesimals into the feeding zone of the core, which increases both its solid and gas component. A fast infall of gas on the core is prevented in this phase by the planetesimal accretion luminosity and by the gravitational energy released by the slow contraction of the envelope. In the core-accretion model, this phase is the longest and it lasts until the so-called crossover mass is reached which is approximately 10–30 $M_{\oplus}$. At this point, the mass of the solid component is approximately equal to that of the gas, and the radiative loss of energy through the envelope overcomes the energy gains, the hydrostatic equilibrium is broken and both planetesimal and gas accretion increase exponentially. However, the gas accumulates at a much faster rate and this runaway gas accretion builds up a massive envelope like that of Jupiter on a short timescale, of the order of a few thousand years. The accretion is finally limited by the rate of gas mass transport from the circumstellar disk towards the planet orbit and, finally, by the disk dispersal after some Myrs. The formation timescales predicted by the original core-accretion model were comparable to or exceeding the lifetime of the circumstellar disks jeopardizing the possibility of forming a significant number of giant planets around stars. However, the formation timescale is significantly reduced if in the model are included: 1) pebble accumulation, which can speed up the solid core accretion phase 2) the core inward migration due to its interaction with the disk, which allows it to access new solid and gas material in all growth phases and 3) the evolution of the opacity of the envelope, which controls its rate of contraction. Fig. 11 illustrates the different stages of the core-accretion model, showing the significant decrease in the formation timescale due to planet migration.

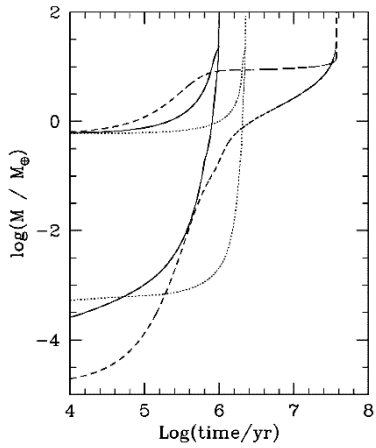

Fig. 11: Growth of Jupiter in different models. For each model the two lines show the mass accreted by solids and gas as a function of time, with the two lines joining at the crossover mass. The dashed line shows a model growing in situ, the dotted line a model with migration starting at 15 *au* from the star, the continuous line a model with the core seed starting at 8 *au* with a slower migration rate compared to the 15 *au* model. In all cases, the initial embryo has a mass of 0.6 $M_\oplus$ (Alibert et al., 2005).

1.9 Structure of the giant planets

Giant planets that form by core-accretion are supposed to have a solid core consisting of a mixture of rock and ice. Present models for the interiors of Jupiter and Saturn, based on available data gathered from space missions and ground observations, predict a core for both planets ranging from a few up to 10–15 Earth masses. However, NASA's Juno spacecraft has measured Jupiter's gravitational field with high accuracy and the data suggest that the core of the planet is not compact but diluted in the inner envelope. A possible way to reconcile this finding with the core-accretion model is, as suggested by Liu et al. (2019), that a massive planetary embryo with a mass approximately of 10 $M_\oplus$ collided head-on with the young Jupiter, shattering its primordial compact core and mixing the heavy elements with the inner envelope of the planet. Such collisions may have been frequent in the early phases of the solar system formation, as suggested by the significant tilts of the rotation axis of Saturn (27°), Uranus (98°) and Neptune (30°). Saturn is less massive than Jupiter, but it

is thought to have a core comparable to that of Jupiter. Within the envelope of hydrogen and helium of the two planets, the hydrogen may become solid at the predicted ultra-high pressures developing deep in the planet atmospheres. The solid hydrogen shows metallic properties where electrons are free to move like those in a metal. This state might explain the strong magnetic field of Jupiter and Saturn due to a combination of free currents and fast rotation rate (see Chapter 3). Saturn also has an additional energy source compared to Jupiter, due to the differentiation of helium from hydrogen, with the former raining out and creating a dense helium-rich layer deep in the interior of the planet. This happens at a significantly lower rate on Jupiter due to convective redistribution of helium in the envelope, which is more effective since Jupiter is warmer than Saturn.

1.10 The icy planets

Uranus and Neptune are referred as icy planets or ice giants, since their composition is probably dominated by water, methane and ammonia ices. They formed at large distances from the sun where the temperatures were low enough to create pebbles and planetesimals that are rich in these ices. They both possess a primordial hydrogen–helium atmosphere, possibly accreted from the circumstellar disk and enriched in methane up to 2%. The methane gives the two planets the classical blue color (methane absorbs red light and reflects blue light). Neptune is about 30% denser than Uranus and is still cooling (it emits approximately 2.7 times the energy it absorbs) due to an excess of heat trapped during the formation process, while Uranus is almost at an equilibrium state with solar radiation. The interior models that fit the data from Voyagers suggest that the planets have a small rocky core made of silicate, iron and nickel, ranging from 0.5 to 3.7 Earth, surrounded by a dense fluid mantle of icy materials under extreme pressure and temperature conditions. It is unclear if in Uranus and Neptune the rocky core is well separated from the ices in the mantle or if they are mixed up in the inner regions of the planets. The fluid mantle has a high electrical conductivity, possibly due to superionic ice. At the pressures and temperatures predicted for the outer layers of the planets, ionized hydrogen atoms are free to move in the oxygen lattice and become conducting charges. This hybrid of solid and liquid is called superionic ice and it is believed it could be the source of the atypical magnetic fields of the two planets (see Chapter 3), which are not parallel to the rotation axis and off-center. One or more impacts with nearby planetary embryos may explain why the spin axis of Uranus is tilted by

about 98^o with respect to the orbital plane. These impacts may also have ejected enough material to create a circumplanetary disk from which some of the Uranian satellites may have formed.

References

Alibert et al., A&A 434, 343–353, 2005
Asphaug & Reufer, Nature Geoscience 7, 564–568, 2014
Barenfeld et al., ApJ 827, 142, 2016
Gullbring et al., ApJ 544, 927, 2000
Kokubo & Ida, The Astrophysical Journal 581, 666–680, 2002
Lambrechts & Johansen, A&A 544, A32, 2012
Liu et al., Nature 572, 355–357, 2019
Mamajek, Proceedings of the International Conference. AIP Conference Proceedings 1158, 3–10, 2009
Ormel & Klahr, A&A 520, A43, 2010
Schneider et al., AJ 125, 1467, 2003
Weidenschilling et al., Icarus 128, 429, 1997
Zsom et al., A&A 513, A57, 2010

2

EXTRASOLAR PLANETS

2.1 The context

An extrasolar planet or exoplanet is, by definition, a planet orbiting a star other than our own. The first exoplanet discovery around a main-sequence star was made by Michel Mayor and Didier Queloz (Nobel prize in 2019) in 1995. They found a giant planet around 51 Pegasi, a sun-like star 4 *Gyr* old located at 50.45 light-years from the Earth. The planet has approximately 0.47 Jupiter masses and it orbits the star in 4.23 days (semi-major axis of about 0.053 *au*). Since then, more than 5,000 new exoplanets have been discovered with different detection methods and their masses range from Earth-like planets to super-Jupiters with masses reaching 20 times the mass of Jupiter, at the planet-brown dwarf borderline. Most of the new planets orbit close to their stars, even if the statistics are incomplete due to observational biases related to the detection methods.

2.2 Detection methods

1) *Radial velocity*. The planet is indirectly detected from the motion of the star around the barycenter of the planet(s)-star system. The absorption lines in the spectrum of the star regularly oscillate due to the Doppler effect (Appendix D.3) caused by the radial velocity of the star with respect to the observer. When the star approaches the observer the light is blue-shifted and when it moves away the light is red-shifted. A radial velocity curve is derived from the spectra taken at different times, like the one derived for 51 Peg and shown in Fig. 1.

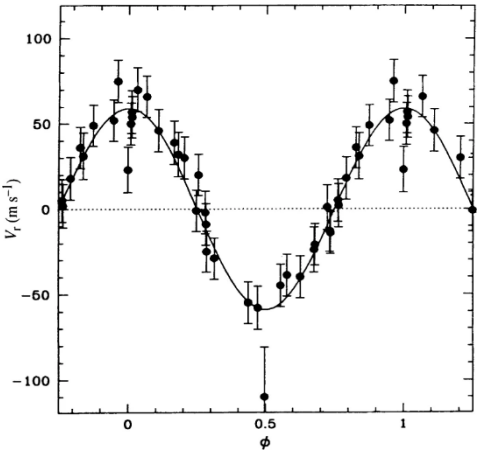

Fig. 1: Radial velocity curve for 51 Peg (Mayor & Queloz, 1995). The solid line is the theoretical interpolation of the data. The phase goes from 0 to 1 and it corresponds to a period of 4.23 *d*.

From the period *T,* the semi-major axis of the planet orbit can be computed with the relationship $T = \frac{2\pi a^{3/2}}{\sqrt{GM_\odot}}$ (see Appendix A). From the semi-amplitude of the radial velocity curve, usually indicated with *K*, it is possible to derive an estimate of the mass of the planet. The planet orbital velocity, in case of circular orbit, can be approximated as $v_{pl} \simeq \sqrt{\left(\frac{GM_\odot}{a}\right)}$ neglecting the mass of the planet and, from the conservation of the momentum, $m_{pl} = M_\odot\, v_\odot / v_{pl}$. Taking into account that *K* is the maximum velocity of the star multiplied by its inclination with respect to the line of sight, we get $m_{pl} = M_\odot\, K/\left(v_{pl} \sin i\right)$. As a consequence, there is an uncertainty in the mass derivation from radial velocity observations, which depends on the inclination of the system with respect to the observer and the extrapolated value is $m_{pl} \sin i$. If the orbit is eccentric, the shape of the radial velocity curve departs from a sinusoid, as shown in Fig. 2, since at the pericenter the planet velocity is higher with respect to the apocenter. In this case, from the fit to the curve it is also possible to derive the eccentricity and the pericenter longitude of the orbit. For young stars, the radial velocity method may misinterpret stellar activity for a planet and a photometric study of the star is needed to confirm the planet detection. The radial velocity method preferentially finds massive planets for which the value of *K* is higher.